Resource-Efficient Technologies 2 (2019) 17–28

TOMSK POLYTECHNIC UNIVERSITY

Resource-Efficient Technologies

journal homepage: http://ojs.tpu.ru/index.php/res-eff

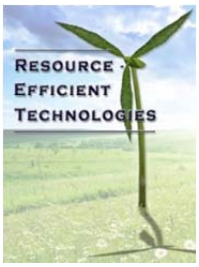

Research Paper

RESOURCE-EFFICIENT METHODS FOR PREDICTING AND SELECTING HEAT-RESISTANT ALLOYS

V.B. Evdokimov[1], A.A. Artamonov[2], E.V. Plotnikov[3]*, N.A. Konstantinova[4]

[1]Limited Liability Company Scientific Production Association Ecohimpribor,
12, Kutuzov Av., Bldg 6, Moscow, 121248, Russia

[2]Research Institute for Space Medicine Federal Research Clinical Center
of Federal Biomedical Agency of Russia,
28, Orechovy Boulevard, Moscow, 115682 Russia

[3]Tomsk National Research Medical Center,
4, Aleutskaya str. Tomsk, 634014, Russia

[4]State Scientific Center of the Russian Federation – Institute of Biomedical Problem of the RAS,
76 A, Khoroshevskoe str. Moscow, 123007, Russia

Abstract

The power plant resource efficiency is largely dependent on heat-resistant alloys and is limited by the standard turbine operating temperature, which is slightly greater than 1000 °C. These temperature limits are dependent on the characteristics of the heat-resistant alloys used in power plants. The current research aimed to discover new heat-resistant alloys using computer-based models to simulate the various properties of such materials. The first-principle methods were initially used in this study. These methods can determine the most important properties of alloys with a high degree of accuracy. This study presented an overview of the software used for first-principle simulation. Using RuAl as the demonstration alloy in this study, we provided step-by-step instructions on how to effectively study the properties of the heat-resistant alloys. Using the first-principle methods, the phonon spectrum and density of the phonon states of B2 RuAl were assessed. We use the parameters of the phonon spectrum to calculate the Grüneisen constant, volume coefficient of thermal expansion, Debye temperature, and temperature dependence of the heat capacity to estimate the melting temperature. Based on the RuAl alloy, the bulk moduli of the elasticity and equilibrium values of lattice parameters were calculated. The simulated results showed good agreement with the experimental data. The calculated parameters of RuAl were compared with those of the NiAl heat-resistant alloy. Using these results, we presented a method for selecting an alloy based on the replacement of ruthenium with nickel in the RuAl alloy. Selection was performed by analyzing the bulk modulus of elasticity and the electron structure of the Ru(Ni)Al alloy.

Keywords: phonon spectrum, density of phonon states, parameters of cell, heat-resistant alloys, Grüneisen constant, thermal expansion, electron structure, resource-efficient technologies

1. Introduction

The energy efficiency and the reliability of power plants are directly correlated with the physical characteristics of the constituent materials in turbines. There is a continuous effort to study and improve the materials used in turbine composition. Due to stringent material requirements necessary to meet the performance standards, the relevance of the work presented in this study is constantly becoming more prevalent. The selection of a highly specialized heat-resistant alloy is a difficult task with significant resource costs due to both material and labor.

* Corresponding author. Tomsk National Research Medical Center, Aleutskaya str. 4, Tomsk 634014 Russia. E-mail address: plotnikov.e@mail.ru

☆ Peer review under responsibility of Tomsk Polytechnic University.
https://doi.org/10.18799/24056537/2019/2/233

Since the 1980s, numerical simulation has been the prevailing resource-efficient method used in the study of such materials. The state-of-the-art simulation enables researchers to solve complex problems regarding solid-state physics. However, a defined scheme used to select heat-resistant alloys (with effective use of software and analysis of the results obtained) is not available. In this review article, the most up-to-date methods and approaches are discussed in detail. In addition, a detailed scheme is presented, providing a means to study all the model stages of the physical properties of heat-resistant alloys using the example of ruthenium and aluminum alloy (RuAl).

The RuAl alloy is of pertinent interest in research due to the rare combination of the following physical properties: high melting point; wide homogeneity range in the high-temperature region [1, 2]; and strength and thermodynamic stability [3–5]. In relation to this, the RuAl alloy is believed to be a promising candidate for the development of a new generation of heat-resistant alloys, with a set of properties superior to those of modern analogs [6–8]. At present, the most common alloys used worldwide are nickel and aluminum-based high-strength alloys (NiAl) due to their suitable mechanical properties that allow them to be used in rocket technology, turbine engineering, and aircraft engineering [9–15] with the B2 structure. However, high demands are required for heat-resistant alloys in these fields; the main demands are high operating temperature and physical strength properties as well as low thermal expansion coefficients [16–18]. At present, efforts are made to increase the temperature of parts made of NiAl-based alloys to obtain empirical evidence. However, the value of the working temperature is close to the limit for NiAl-based alloys. Currently, it is possible to increase the temperature on the surface of a blade (as an example) due to new channel configurations for penetrating cooling as well as protective coatings [16, 19, 20]. The blades are prepared using single crystals using composites with special technological solutions [21–27], resulting in the improvement of some of the technical characteristics of the blades. The cost of the blades is up to half the cost of the power unit.

Moreover, despite the high density and cost, the RuAl intermetallic alloy can help solve the problem presented by increasing the working temperature. Alloys with a high ruthenium content have the physical advantages of extremely high toughness, high creep resistance, and low-temperature value of plastic flow stress. Compared to NiAl, the RuAl alloy has a higher melting point. In addition, RuAl has a lower thermal expansion coefficient [28], which is an important parameter since it reduces the mechanical stress when working within a large temperature range. These aforementioned physical qualities must be considered when searching for new alloys. Moreover, up-to-date technological methods of simulation must be used to conduct preliminary searches for new alloys. All alloys based on Al and modifications of the NiAl alloy can be considered as promising alloys.

Relevant research materials are extremely expensive and present with some technological difficulties. Some characteristics of alloys cannot be fully investigated, which creates the need for numerical calculations. Such calculations make it possible to thoroughly cover numerous physical parameters and material conditions that would otherwise be empirically inaccessible. A considerable number of research pertaining to the thermodynamic and mechanical properties of RuAl and other alloys based on RuAl has been carried out [28–34]. The initial steps in the study of the physical properties of the RuAl intermetallic compound include the calculation of the electron structure and equilibrium parameters of the alloy. These calculations are then compared with the experimental results. This stage presents a platform for further theoretical study of the alloy's thermodynamic properties (such as temperature dependence). In this research, understanding of the dynamics of the RuAl alloy's crystal lattice was emphasized.

2. Materials and Methods

The density functional theory (DFT) [35–39] was used to calculate the following: total energy of the system, lattice parameter, dispersion law, electron density distribution, and density of states. The search for the cell parameter's equilibrium value was found after assessing the total system's energy dependence on the cell parameter. The total energy of the system was described using equation [40]:

$$E_{tot} = E_{I-I} + T_0[n] + E_{e-i} + E_{e-e} + E_{xc}, \quad (1)$$

where E_{tot} is the total energy, E_{I-I} is the ion–ion interaction energy, $T_0[n]$ is the electron kinetic energy, E_{e-i} is the electron–ion interaction energy, E_{e-e} is the electron–electron interaction energy, and E_{xc} is the exchange–correlation energy. To determine the equilibrium lattice parameter, it is necessary to construct

the dependence of the total energy on the lattice parameter and to find the minimum energy value. The equilibrium lattice parameter corresponds to the minimum energy [12]. The equation for the dependence of the energy of the lattice on the lattice parameter usually has the form of a quadratic equation**.**

At this stage, it is possible to compare the discovered value of the lattice parameter with the experimentally obtained value. For such calculations, a high accuracy is required, making it necessary to vary the parameters in the search of the most optimal values. The accuracy criterion must be during a convergence in energy while at optimal resolution (accurate up to sixth decimal place). Such accuracy allows us to consider the mixing energy. The basic functions are plane waves with a maximum energy of 30 Ry. Fourier charge density components were used with an energy less than 750 Ry. Regarding integration over the Brillouin zone, a grid of *k*-points (with a minimum of 16×16×16) should be used, whereas summation over zones must be carried out using the first-order Gauss–Hermite function of 10-mRy width [41]. To generate and carry out the inverse Fourier transform of the matrix of power constants, a set of 6×6×6 q-points was used. The implemented pseudopotentials were ultra-soft (USP). All calculations were carried out using the Plane-Wave Self-Consistent Field (PWSCF) package via Quantum-ESPRESSO [42–45].

The authors warn that this method has a limitation – the temperature is artificially introduced into the calculations (by varying the volume of the unit cell). However, this does not interfere with prediction of the physical properties of the alloy with great accuracy.

3. Results and Discussion

The analysis pertaining to lattice dynamics is based on the understanding of phonon oscillations and their features in a given case. Experimental studies of phonon oscillations are extremely difficult to conduct [46]. At this stage, it is necessary to use computer-based simulations. In our example, we used the PWSCF quantum computing package described above (Quantum-ESPRESSO). Fig. 1 shows the phonon spectrum obtained from the simulation. The gap between the optical and acoustic branches is visible on the dispersion plot (Fig. 1). The gap width is 57 cm^{-1}. The gap arises as a result of the separation of optical and acoustic branches due to the difference in atomic masses ($M_{Ru}/M_{Al} \approx 4$). The upper optical branches of vibrations are associated with light aluminum atoms. The crystallographic directions GX, GM, and GR correspond to a degenerate transverse mode with two directions of the polarization vector perpendicular to the wave vector as well as a non-degenerate longitudinal mode. In the direction of XM, symmetry does not lead to degeneration, and three modes are separated. In the direction of XM, GM, and/or MR, the frequency of longitudinal oscillations is lower than the frequency of the transverse wave. This corresponds to a situation when longitudinal vibrations in the substance are compressed and stretched by a quasi-elastic force. This quasi-elastic force is smaller than the force leading to the bending associated with transverse waves. When the spectrum of phonon oscillations is obtained, it is possible to determine whether the lattice is stable or unstable by noting the absence of negative phonon frequencies. If negative phonon oscillations are detected, then it can be said with certainty that the lattice is unstable and that the lattice type (or its parameters) was found incorrectly. It is also possible to trace the lattice stability using phonon oscillations at different pressures and temperatures (assuming that specific temperature threshold leads to a certain expansion of the material).

An important parameter characterizing lattice dynamics is the Grüneisen constant [47]. This constant can be used to estimate the melting point of a potential alloy as well as its thermal expansion.

To determine the values of the microscopic Grüneisen constant $\gamma(jk)$, the following equation was used:

$$\gamma(jk) = -\frac{\partial \ln(\varpi(jk))}{\partial \ln V}, \tag{2}$$

which took the following form after simplification:

$$\gamma(jk) = -\frac{V_0 \Delta\varpi(jk)}{\varpi_0(jk)\Delta V}, \tag{3}$$

where $\Delta\varpi(jk)$ is the frequency difference of phonon oscillations calculated for each k value at equilibrium volume V_0 and a volume larger by 2.7 %.

Fig. 2*a* shows the Grüneisen constant for various crystallographic directions. It is worth noting that in the crystallographic direction G (for the acoustic branch of TA2), the Grüneisen constant is negative. That is, in this direction, we can expect a minimum thermal expansion of the alloy.

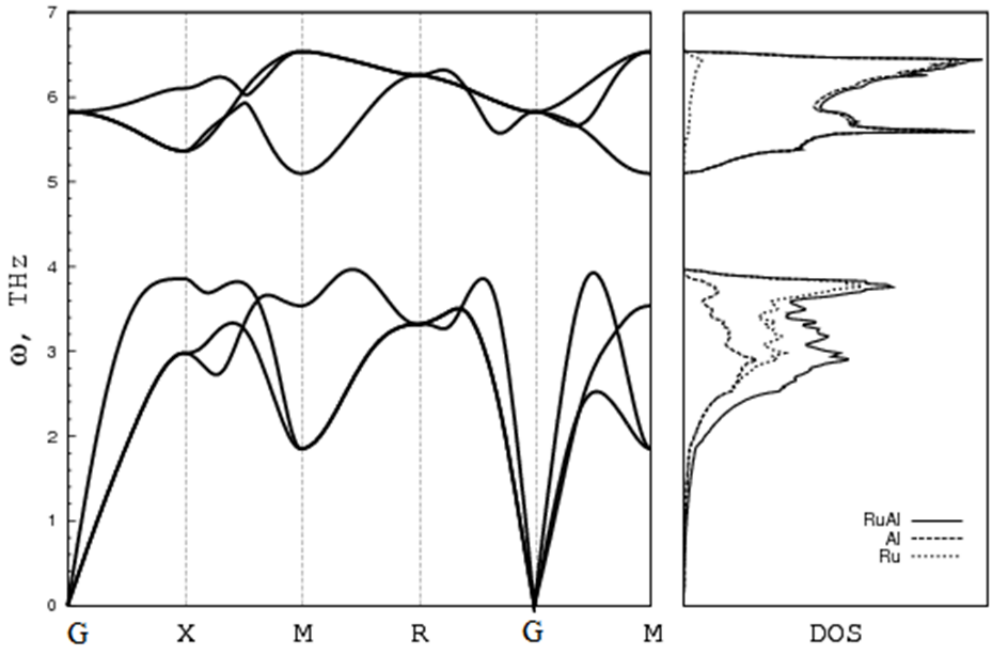

Fig. 1. The left part of the figure is the spectrum of phonon oscillations. The upper spectrum refers to the optical part of the phonon oscillations, and the lower spectrum refers to the acoustic part of the oscillations. The right part of the figure is the plot of the density of phonon states (DOS), where the partial contribution of Ru and Al to the total density of phonon states (RuAl) is highlighted

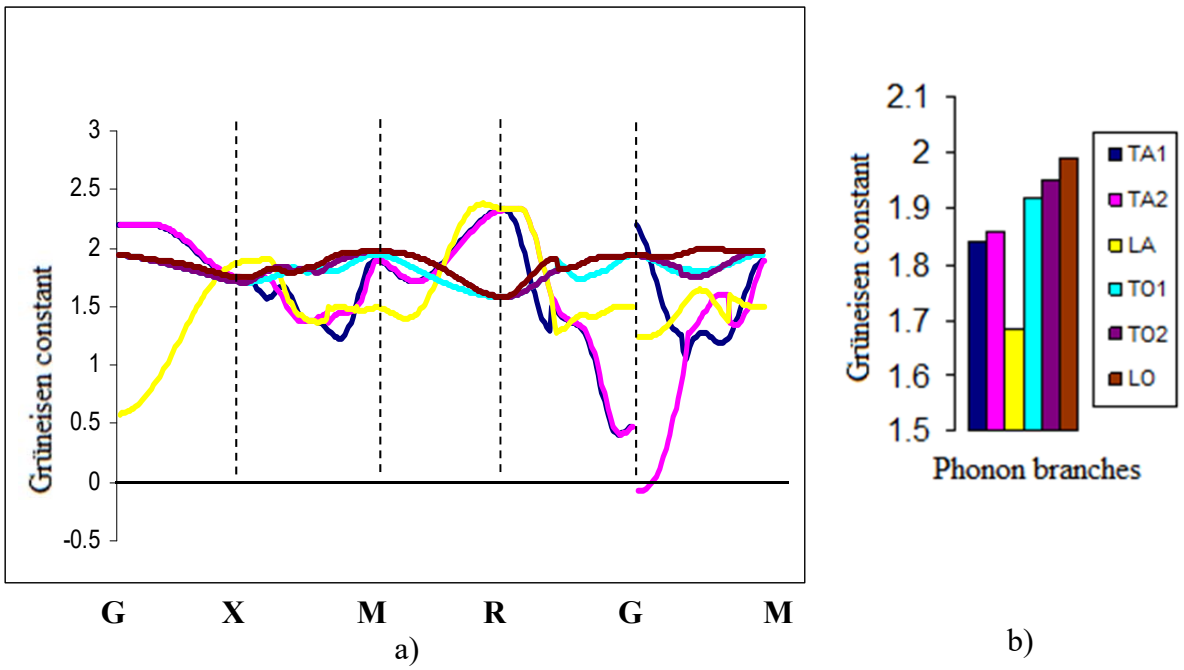

Fig. 2. a) Microscopic values of the Grüneisen constant for all the branches of the phonon oscillations. b) Value of the Grüneisen constant for individual phonon branches: TA1 and TA2 (TO1 and TO2) are two transverse acoustic (optical) branches, and LA (LO) is a longitudinal acoustic (optical) branch. The colors of the branches on the right and left figure are similar

Then, in the Einstein approximation [48], the mean value of the Grüneisen constant γ_G was found using the following equation:

$$\gamma_G = \frac{1}{n}\sum\gamma(jk), \quad (4)$$

where n is the number of the k-vectors used.

Thus, the average value of the constant γ_G was 1.72. Fig. 2*b* shows the contribution of each phonon branch to the value of the Grüneisen constant. Acoustic branches make a smaller contribution than optical branches, since the latter can appear as a result of vibrations within the lighter aluminum. The Grüneisen constant used to compare the results was

also calculated using the Debye temperature [48–50].

For 15 different volumes (seven on the right and seven on the left of the non-equilibrium volume parameters, with a step of 2.7 % from central equilibrium volume parameter whish was include also), the Debye temperature was calculated; the Grüneisen constant was determined using the following equation:

$$\gamma(jk) = -\frac{\partial \ln(\Theta_D)}{\partial \ln V}. \quad (5)$$

This method results in a value of 1.66. The approximate relationship between the high-temperature value of the Grüneisen constant is γ_{HT} and the low-temperature value is γ_{LT}. This relationship is defined as follows:

$$\gamma_{HT} - \gamma_{LT} \approx \frac{1}{3}. \quad (6)$$

According to this equation, the value of the Grüneisen constant at high temperature can be estimated as follows:

$$\gamma_{HT} \approx 2.05$$

Since the constant $\gamma(jk)$ was calculated for both acoustic and optical branches, we can estimate the contribution made by optical phonons to the value of the Grüneisen constants to as follows:

$$\gamma_A = 1.60,\ \gamma_{A+O} = 1.72,$$

where γ_A is the value taking into account the acoustic branches, and γ_{A+O} is the value taking into account the acoustic and optical modes. As a result of switching on the optical modes, the Grüneisen constant increases by 7.5 %.

The Grüneisen constant found using the above-mentioned method was 1.42 (for NiAl). If the constant for NiAl is compared to that of RuAl, it is discerned that nickel aluminate has a smaller constant. This difference is due to the fact that ruthenium atoms are heavier than nickel atoms.

Knowing the value of the bulk modulus of elasticity and the Grüneisen constant, one can find the coefficients using the Morse formula [51] for an approximate calculation of the total energy depending on the lattice parameter:

$$E_{tot} = A - 2D * e^{-\lambda(r-r0)} + D * e^{-2\lambda(r-r0)} \quad (7)$$

$$\lambda = \frac{2\gamma_G}{r_0}, \quad (8)$$

$$r_0 = -\frac{\ln(x_0)}{\lambda},$$

$$B(r_0) = -\frac{cx_0^2\lambda^3}{6\pi \ln(x_0)},$$

$$x_0 = \frac{-b}{2c},\ x = e^{-\lambda r},$$

$$D = \frac{b^2}{4c}.$$

From equations (8), we identified the unknown parameters λ and D.

λ, a.u.$^{-1}$	D, Ry
0.651	1.024×10^{-3}

It is worth noting that despite their empirical validity, the calculations carried out in equations (7) and (8) can accurately estimate the dependence of lattice energy on its parameter, which can then be compared with the results of the simulation carried out for equation (1).

Another important relation, the Debye temperature–temperature is determined by evaluating the simulation results. Figs. 3*a* and 3*b* show this dependence for the RuAl alloy. As a rule for high-temperature alloys, the Debye temperature is interesting at alloy temperatures of more than 1000 K, where the Debye temperature is already weakly dependent on the temperature of the alloy. Nevertheless, the experimental determination of the Debye temperature is possible at low temperatures. Therefore, the entire temperature range is simulated to accurately determine this dependence.

When T<40 K, the curve has a common shape. The Debye temperature first decreases with increasing T and then passes through a minimum. If the oscillations were strictly harmonic, then one would expect the curve to be flatter at higher temperatures. The reason for the constant increase – which can be observed up to 150 K – is due to the anharmonic contribution. At higher temperatures, the characteristic temperature value is more likely to be approximately 528 K. NiAl alloy has a lower Debye temperature (462 K). Since the numerical values of the characteristic temperatures differ from each other, it is necessary to bring them to a form that is convenient for comparison. Fig. 4 shows two temperature dependencies for RuAl and NiAl. The abscissa axis shows the values T/Θ_D^0, and the ordinate axis represents the ratio Θ_D/Θ_D^0, where Θ_D^0 is the Debye temperature at 0 K.

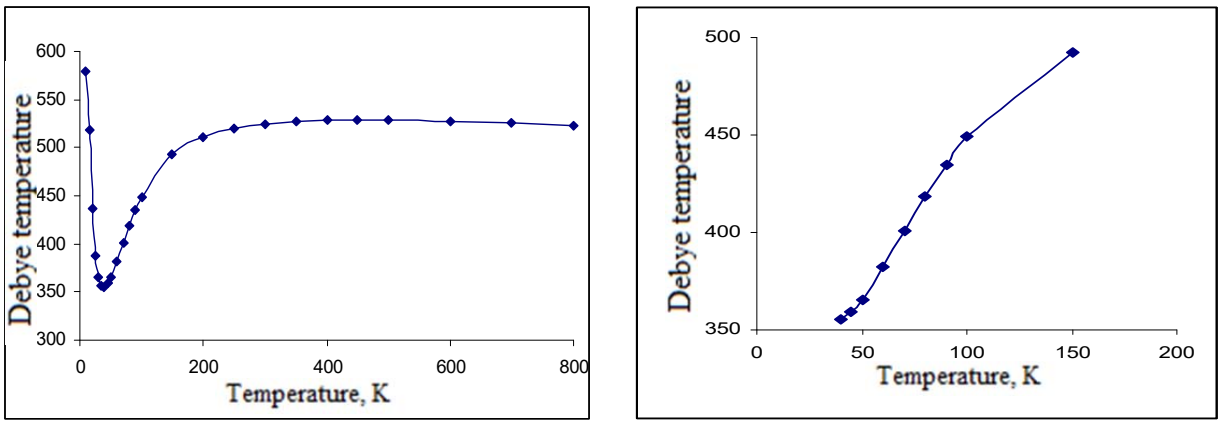

a) b)

Fig. 3. a) Temperature dependence of the Debye temperature in the temperature range of 0–800 K; b) Part of the dependence of the Debye temperature in the range of 40–150 K

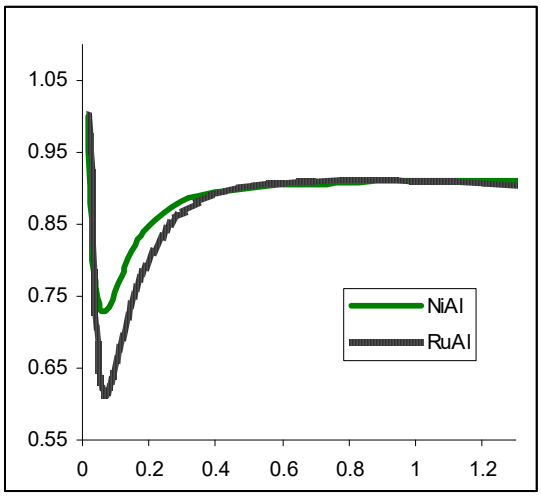

Fig. 4. Temperature dependence of the Debye temperature

The steepness of decreasing $\Theta_D(T)$ with increasing temperature from 0 K corresponds to the speed of deviation of the actual frequency distribution from the Debye distribution. The minimum depth indicates the magnitude of this deviation. After analyzing the type of dependence in Fig. 4, it can be concluded that the observed types of frequency distribution are similar, but the numerical value of the mode density differs. Knowing this value, one can find the average value of the second moment of the frequency $\overline{\nu^2}$ of phonon oscillations using the following equation:

$$\Theta_D = \sqrt{\frac{5}{3} * \overline{\nu^2}}\,. \tag{9}$$

The result of calculations is $\overline{\varpi^2} = 7.22 * 10^{25}\,\mathrm{s}^{-2}$, with the second moment frequency value found using the phonon spectra: $\overline{\varpi^2} = 4.037 * 10^{25}\,\mathrm{s}^{-2}$.

It is also reasonable to calculate the speed of sound using the following equation:

$$\varpi_D = \left(\frac{6\pi^2 N}{V}\right)^{1/3} c\,, \tag{10}$$

where c is the speed of sound, V is the crystal volume, and N is the total number of modes.

The speed of sound (obtained from model calculations) is equal to 2.337×10^5 m/s. The calculated speed of sound can be compared with the experimental value, which enables us to check the accuracy of the calculation.

Another important quantity that can be experimentally tested is heat capacity.

By measuring the heat capacity, it is possible to obtain additional information regarding lattice dynamics [51–56], which can then be compared to existing data.

Heat capacity is obtained using the following equation:

$$C_V = \left(\frac{\partial E}{\partial T}\right)_V = $$

$$= k_B \sum_{kj} \left[\frac{\hbar\varpi(kj)}{k_B T}\right]^2 \frac{\exp\left\{\frac{\hbar\varpi(kj)}{k_B T}\right\}}{\left(\exp\left\{\frac{\hbar\varpi(kj)}{k_B T}\right\} - 1\right)^2}\,. \tag{11}$$

At room temperatures, the heat capacity is close to $3\,Nk_B \approx 6$ cal/mol×K, where N is the total number of modes. The dependence of the heat capacity on temperature in the intervals from 0 to 60 K [from equation (10)] is well approximated using the cubic equation

$$C_V(T) = 4\cdot10^{-6}T^3 + 3\cdot10^{-3}T\,. \tag{12}$$

The numerical coefficient at T^3 can be predicted with fairly good accuracy using the equation

$$\Theta_0 = \left(\frac{12\pi^4 Nk}{5a} \right)^{1/3}, \quad (13)$$

where Θ_0 is the Debye temperature at 0 K, the numerical value (in our case) is 579 K, N is the number of atoms, k is the Boltzmann constant, and a is the coefficient in equation (11) at T^3. The value obtained using equation (12), $a = 2.394\times10^{-6}$ cal/mol×K^4, is slightly different from the value provided by equation (13) due to the fact that we took the value of Θ_0 at 2 K (instead of zero). However, this still shows a good agreement with the calculated results. In the approximation equation, the electron's contribution to the heat capacity γ_e can be found as the coefficient before T. The value $\gamma_e=3\times10^{-3}$ cal/mol×K^2 is not large due to the small density of electronic states at the Fermi level. Since the dependence of heat capacity on temperature is known, it is possible to estimate the zero-oscillation energy. Oscillatory energy is defined as the sum of zero and thermal oscillation energy.

Thermal energy is defined as $E_T = \int_0^T C_V dT$; according to $C_V(T)$, a graph of $E_T(T)$ can be plotted.

By contrast, at high temperatures, thermal energy can be represented as follows:

$$E_T = -E_Z + 3NkT\left[1 + \frac{1}{2!}|B_2|\overline{\varpi^2}\left(\frac{h}{kT}\right)^2 - \ldots \right], \quad (14)$$

where E_T is the thermal energy, E_Z is the zero-oscillation energy, B_n is the Bernoulli numbers, $\overline{\varpi^2}$ is the moment, N is the total number of modes, h is the Planck constant, k is the Boltzmann constant, and T is the temperature.

If the temperature is high, the term in square brackets approaches unity. As a result, the plot of E_T versus temperature will be a straight line. The segment cut off by the extension of this straight line at $T = 0$ will be equal to E_Z.

The calculations provide the value of $E_Z = 0.00544$ Ry per cell (for RuAl alloy). This value is slightly different from the value calculated directly from the phonon spectrum – $E_Z = 0.00654$ Ry per cell – for NiAl $E_Z = 0.00633$ Ry per cell. The abovementioned can help us to check and compare obtained results at each stage of calculation. Verification of results is one of the tasks, and the solution of which will ensure that the modeling is carried out effectively.

It is also possible to estimate the heat of sublimation ΔH_{sub} (at 0 K), knowing the static energy of the lattice (E_0), which is calculated as a result of a self-consistent calculation:

$$E_0 = -E_Z - \Delta H_{sub}. \quad (15)$$

In equation (15), we find that the heat of sublimation ΔH_{sub} (at 0 K) is equal to 204.31 Ry per cell. Since zero oscillations occur even at temperatures comparable to 0 K, an expansion of the lattice associated with these oscillations also occurs, and it is defined by equation (16):

$$\frac{\Delta V}{V(0^0 K)} = \frac{\chi_T(0^0 K)}{V(0^0 K)} \gamma_G E_Z, \quad (16)$$

where $V(0^0\ K)$ is the lattice volume at 0 K and $\chi_T(0^0\ K)$ is the compressibility index of the lattice.

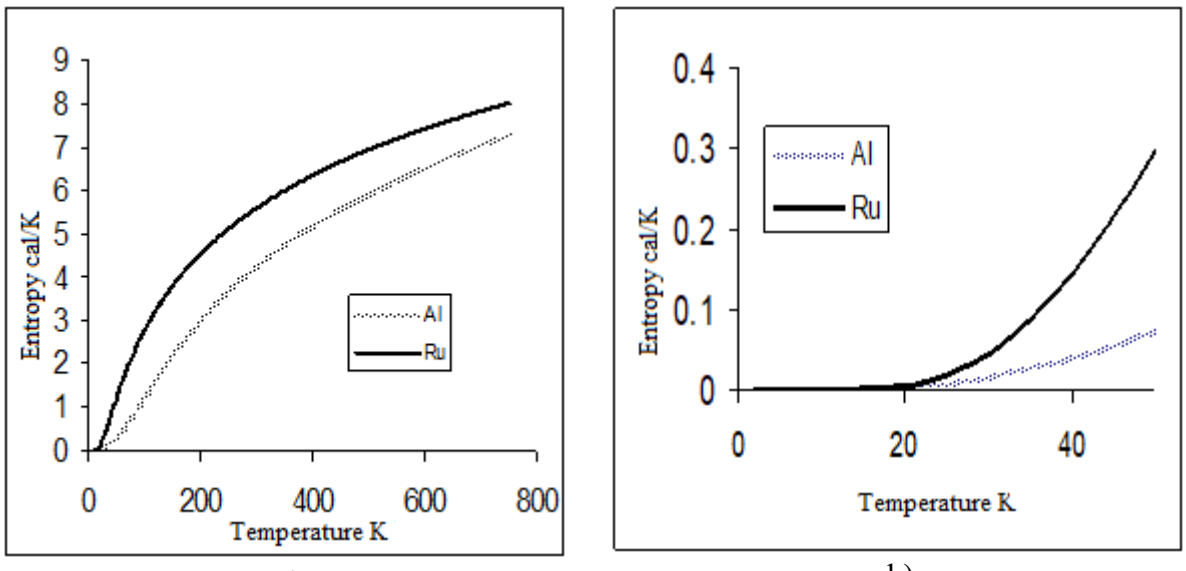

a) b)

Fig. 5. a) Partial entropy versus temperature; b) Partial entropy in the temperature range from 2 to 60 K

The volumetric expansion of the lattice as a result of zero oscillations is 0.43 %.

The form of dependence in Fig. 5*a*–5*b* reflects the entropy contribution from each element of the RuAl alloy. Ruthenium makes a greater contribution to the entropy due to its mass. As mentioned previously, the mass of ruthenium is about 4 times greater than that of aluminum. Ruthenium is less mobile than aluminum, which affects the oscillation properties, as depicted in Table 1.

Table 1. Partial contribution of Ru and Al as well as Ni and Al to the energy of zero oscillations and phonon density of states in RuAl and NiAl alloys, respectively

Element	Partial contribution to zero-oscillation energy, Rydberg/atom	Partial contribution to the phonon density of states
Al (RuAl)	0.005430	3.374703
Ru (RuAl)	0.001659	2.628610
Al (NiAl)	0.001875	2.550468
Ni (NiAl)	0.004454	3.450039

In the NiAl alloy, there exists a reverse situation. That is, Ni makes a greater contribution to the oscillations and phonon density of states.

An important characteristic of heat-resistant materials is thermal expansion. In this study, the coefficient of thermal expansion was determined experimentally for the RuAl alloy [57–61]. The coefficient of volume thermal expansion is in a wide temperature range (from 400 to 1773 K), and the boundary values of thermal expansion are 5.5×10^{-6} K^{-1} and 11×10^{-6} K^{-1}, respectively. Such low value can be explained by the weak contribution of lattice oscillations to thermal expansion. The advantage of using quantum modeling as a research method is that it can estimate the coefficient of thermal expansion under conditions that are not available experimentally.

In this work, thermal expansion was determined using the phonon spectrum. The value of the thermal expansion coefficient was 7.2×10^{-6} K^{-1} at a temperature of 400 K and 8.7×10^{-6} K^{-1} at 1773 K, respectively.

It is possible to estimate the coefficient of volumetric thermal expansion when knowing the elastic modulus and Grüneisen constant:

$$\alpha = \frac{2k\gamma}{BV}, \tag{17}$$

where k is the Boltzmann constant, γ is the Grüneisen constant, B is the bulk modulus of elasticity, and V is the cell volume.

This method of evaluation gives the value of $\alpha=8.5\times10^{-6}$ K^{-1}.

If we assume that the oscillation and electron contribution to the volume expansion is additive, we can separate these terms to find numerical values. It is enough to straighten $\frac{\alpha(T)}{T}$ from T^2 in the following coordinates:

$$\alpha(T) = \zeta T + \xi T^3, \tag{18}$$

where $\zeta=10^{-8}$ K^{-1} is the electron contribution and $\xi=9\times10^{-13}$ K^{-3} is the contribution of oscillations.

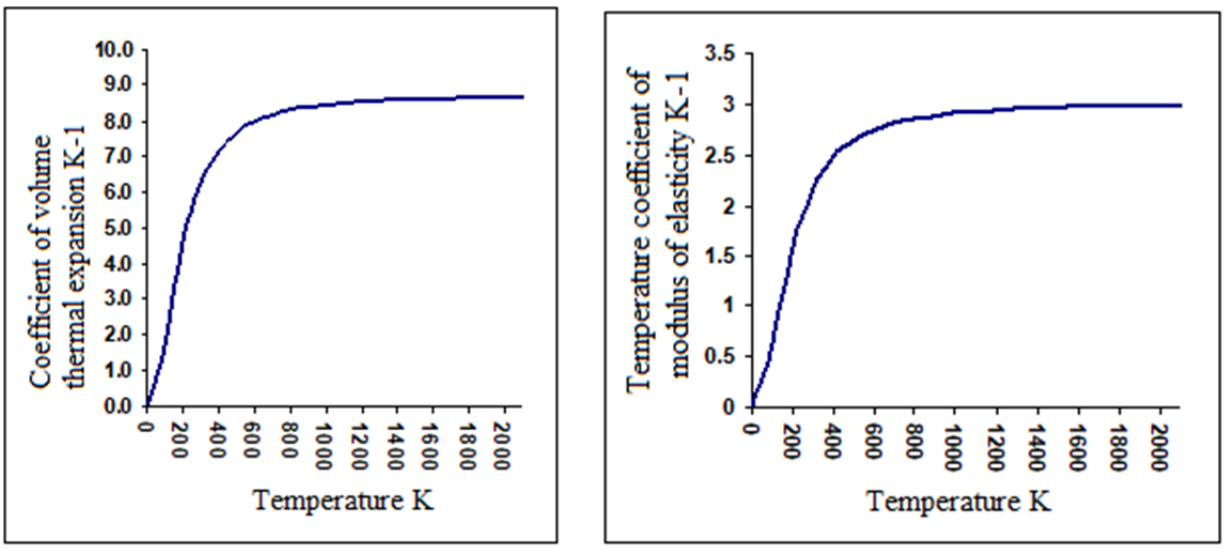

a) b)

Fig. 6. a) Coefficient of volume thermal expansion ×10^6 vs temperature.
b) Temperature coefficient of the modulus of elasticity ×10^5 vs temperature

Fig. 6*a* shows the thermal expansion coefficient's dependence on temperature. The relationship between the thermal expansion coefficient and the temperature coefficient of the modulus of elasticity is given in the equation

$$\alpha_B(T) = 2\gamma\alpha_V(T), \quad (19)$$

where $\alpha_B(T)$ is the temperature coefficient of the modulus of elasticity and $\alpha_V(T)$ is the coefficient of volume thermal expansion.

The calculated view of the temperature coefficient dependence of the elasticity modulus on temperature is shown in Fig. 6*b*.

The obtained model dependence of the bulk modulus of elasticity on temperature can be compared with the experimental values [62–66].

A very important characteristic of a heat-resistant material is inherent melting point. There are several semi-empirical methods for estimating the melting point. A way to estimate the lower limit of the melting point through the Debye temperature is as follows:

$$T_L > \frac{T_D}{0.3}. \quad (20)$$

The lowest limits of the melting point are 1927 K for RuAl and 1540 K for NiAl. The melting points (found using the abovementioned method) are in good agreement with the experimental values [67, 68]. The high melting point of the RuAl alloy distinguishes it from all other high-temperature alloys.

4. Conclusion

The prediction methods used in this study are in good agreement with experimental data, and they can be used to develop new alloys. The resource-efficient scheme for determining the physical properties of alloys presented in this paper makes it possible to optimize the use of computational and material resources associated with experiments. This scheme can be supplemented with other systems when evaluating alloys, simulating corrosion characteristics, or applying the theory of physicochemical analysis to alloys [69–71]; this includes cases of unstudied alloys. It is also possible to directly take into account temperature effects when conducting quantum calculations given that the thermodynamic uncertainty relation [72, 73] is considered when performing such calculations.

Acknowledgments

The authors are grateful to the staff of the Department of Theoretical Physics and Quantum Technologies of MISIS E.I. Isaev, Yu.Kh. Vekilov, and I.D. Bleskov for valuable comments and discussion of the results.

References

[1] Obrowski W. Alloys of ruthenium with boron, beryllium and aluminium. *Metall*, 1963, vol. 17, no. 2, p. 108–112.

[2] Tryon B., Feng Q., Pollock T. Intermetallic phases formed by ruthenium–nickel alloy interdiffusion. *Intermetallics*, 2004, vol. 12, no. 7–9, pp. 957–962. doi: 10.1016/j.intermet.2004.02.026.

[3] Tryon B., Pollock T.M., Gigliotti M.F.X., Hemker K. Thermal expansion behavior of ruthenium aluminides. Scripta Materialia, 2004, vol. 50, no. 6, pp. 845–848. doi: 10.1016/j.scriptamat.2003.12.009.

[4] Ying W. Manufacturing and microstructure RuAl/NiAl diffusion barrier coating for Ni-based crystal superalloy substrate, 2007, *6th International Conference on Materials Processing for Properties and Performance*, Rome, Italy.

[5] Bleskov I.D., Smirnova E.A., Vekilov Y.K., Korzhavyi P.A., Johansson B., Katsnelson M., Isaev E.I. Ab initio calculations of elastic properties of $Ru_{1-x}Ni_xAl$ superalloys. *Applied Physics Letters*, 2009, vol. 94, article number 161901. doi: 10.1063/1.3120543.

[6] Povarova K.B., Padalko A.G., Drozdov A.A., Kasanskaya N.K., Korenovskii N.L., Skachkov O.A., Veselov A.N., Morozov A.E., Bannykh I.O. Differential barothermal analysis in the course of reactive powder barothermal processing of RuAl alloys. *Journal of thermal analysis and calorimetry*, 2005, vol. 80, no. 3, pp. 607–612. doi: 10.1007/s10973-005-0701-y.

[7] Wolff I.M., Hill P.J. Platinum metals-based intermetallics for high-temperature service. *Platinum Metals Review*, 2000, vol. 44, no.4, pp. 158–166.

[8] Cornish L.A., Süss R., Watson A., Prins, S.N. Building a thermodynamic database for platinum-based superalloys: Part I. *Platinum Metals Review*, 2007, vol. 51, no. 3, pp. 104–115. doi: 10.1595/147106707X212967.

[9] Nazarkin R.M., Kolodochkina V.G., Ospennikova O.G., Orlov M.R. The microstructure modifications of single crystals of Ni-based superalloys in time-tested turbine blades. *Aviation materials and technology*, 2016, no. 4(45), pp. 9–17. doi: 10.18577/2071-9140-2016-0-4-9-17. In Russian.

[10] Kablov E.N., Petrushin N.V., Svetlov I.L. Demonis I.M. (2012). Ni-base casting superalloy of the new generation. *Aviation materials and technology*, 2012, no. 8, pp. 36–51. In Russian.

[11] Darolia R. NiAl alloys for high-temperature structural applications. *JoM*, 1991, vol. 43, no. 3, pp. 44–49. doi: 10.1007/BF03220163.

[12] Bleskov I.D., Isaev E.I., Vekilov Y.K. Electronic structure and ground state parameters of $Ru_{1-x}Me_xAl$ refractory alloys. *Physics of the Solid State*, 2010, vol. 52, no. 9, pp. 1803–1809. doi: 10.1134/S1063783410090039.

[13] Darolia R. Ductility and fracture toughness issues related to implementation of NiAl for gas turbine applications. *Intermetallics*, 2000, vol. 8, iss. 9–11, pp. 1321–1327. doi: 10.1016/S0966-9795(00)00081-9.

[14] Hamadi S., Bacos M.P., Poulain M., Seyeux A., Maurice V., Marcus P. Oxidation resistance of a Zr-doped NiAl coating thermochemically deposited on a nickel-based superalloy. *Surface and Coatings Technology*, 2009, vol. 204, no. 6–7, pp. 756–760. doi: 10.1016/j.surfcoat.2009.09.073.

[15] Pascal C., Marin-Ayral R.M., Tedenac J.C. Joining of nickel monoaluminide to a superalloy substrate by high pressure self-propagating high-temperature synthesis. *Journal of Alloys and Compounds*, 2002, vol. 337, no. 1–2, pp. 221–225, doi: 10.1016/S0925-8388(01)01924-7.

[16] Kablov E.N., Ospennikova O.G., Petrushin N.V. New single-crystal intermetallic high-temperature alloy based on γ′-phase for GTE blades. *Aviation materials and technologies*, 2015, no. 1(34), pp. 34–40. doi: 10.18577/2071-9140-2015-0-1-34-40. In Russian.

[17] Ospennikova O.G. Trends in the creation of low-density heat-resistant nickel alloys with polycrystalline and single-crystal structure (review). *Aviation materials and technology*, 2016, no. 1(40), pp. 3–19. doi: 10.18577/2071-9140-2016-0-1-3-19. In Russian.

[18] Bazyleva O.A., Ospennikova O.G., Arginbaeva E.G., Letnikova E.Yu., Shestakov A.V. Development trends of nickel-based intermetallic alloys. *Aviation materials and technology*, 2017, no. 5, pp. 104–115. doi: 10.18577/2071-9140-2017-0-S-104-115. In Russian.

[19] Kablov E.N., Ospennikova O.G., Svetlov I.L. Highly efficient cooling of GTE hot section blades. *Aviation materials and technologies,* 2017, no. 2 (47). doi: 10.18577/2071-9140-2017-0-2-3-14. In Russian.

[20] Petrushin N.V., Ospennikova O.G., Svetlov I.L. Single-crystal Ni-based superalloys for turbine blades of advanced gas turbine engines. *Aviation materials and technology*, 2017, no. S, pp. 72–103. doi: 10.18577/2071-9140-2017-0-S-72-103. In Russian.

[21] Jureczko M., Pawlak M., Mężyk A. Optimisation of wind turbine blades. *Journal of Materials Processing Technology*, 2005, vol. 167, no. 2–3, pp. 463–471, doi: 10.1016/j.jmatprotec.2005.06.055.

[22] Brøndsted P., Lilholt H., Lystrup A. (2005). Composite materials for wind power turbine blades. *Annual Review of Materials Research*, vol. 35, pp. 505–538. doi: 10.1146/annurev.matsci.35.100303.110641.

[23] Gell M., Duhl D.N., Giamei A.F. The development of single crystal superalloy turbine blades. *Superalloys*, 1980, pp. 205–214. doi: 10.7449/1980/Superalloys_1980_205_214.

[24] Veers P.S., Ashwill T.D., Sutherland H.J., Laird D.L., Lobitz D.W., Griffin D.A., Miravete A. Trends in the design, manufacture and evaluation of wind turbine blades. *Wind Energy*, 2003, vol. 6, no. 3, pp. 245–259, doi: 10.1002/we.90.

[25] Thomsen O.T. Sandwich materials for wind turbine blades – present and future. *Journal of Sandwich Structures and Materials*, 2009, vol. 11, no. 1, pp. 7–26. doi: 10.1177/1099636208099710.

[26] Müller J., Neuschütz D. Efficiency of α-alumina as diffusion barrier between bond coat and bulk material of gas turbine blades. *Vacuum*, 2003, vol. 71, no. 1–2, pp. 247–251. doi: 10.1016/S0042-207X(02)00746-7.

[27] Mandell J.F., Samborsky D.D., CAIRNS D. *Fatigue of Composite Materials and Substructures for Wind Turbine Blades*; TOPICAL, Report no. SAND--2002-0771, Sandia National Labs, 2002, 264 p.

[28] Guitar M.A., Mücklich F. Isothermal oxidation behaviour of nanocrystalline RuAl intermetallic thin films. *Oxidation of Metals*, 2013, vol. 80, no. 3–4, pp. 423–436. doi: 10.1007/s11085-013-9409-8.

[29] Borah A., Robi P.S., Srinivasan A. Synthesis of nanocrystalline RuAl by mechanical alloying. *Metals and Materials International*, 2007, vol. 13, no. 4, pp. 293–302. doi: 10.1007/BF03027885.

[30] Povarova K.B., Morozov A.E., Skachkov O.A., Drozdov A.A., Kazanskaya N.K., Korenovskii N.L., D'yakonova N.B. Effect of mechanical activation on the characteristics of ruthenium and aluminum powder mixtures. *Russian Metallurgy (Metally)*, 2008, no. 3, pp. 232–238. doi: 10.1134/S0036029508030099.

[31] Tryon B., Cao F., Murphy K.S., Levi C.G., Pollock T.M. Ruthenium-containing bond coats for thermal barrier coating systems. *JoM*, 2006, vol. 58, no. 1, pp. 53–59. doi: 10.1007/s11837-006-0069-x.

[32] Bleskov I.D., Isaev E.I., Vekilov Yu.Kh. Electronic structure and ground parameters of Ru1-xMexAl refractory alloys. *Physics of the Solid State*, 2010, vol. 52, no. 9, pp. 1803–1809. doi: 10.1134/S1063783410090039.

[33] Borah A., Robi P.S., Mujumdar A.L., Srinivasan A. Microstructural evolution and hardening behaviour of cast and heat-treated Ru−Al and Ru−Al−Ni alloys. *Metals and Materials International*, 2008, vol. 14, no. 1, pp. 123–132. doi: 10.3365/met.mat.2008.02.123.

[34] Kablov E.N. Innovative developments of FSUE "VIAM" SSC RF in realization of Strategical directions of development of materials and technologies of their processing for period up to 2030 year. *Aviation materials and technologies*, 2015, no. 1(34), pp. 3–33. doi: 10.18577/2071-9140-2015-0-1-3-33. In Russian.

[35] Brandbyge M., Mozos J.L., Ordejón P., Taylor J., Stokbro K. Density-functional method for nonequilibrium electron transport. *Physical Review B*, 2002, vol. 65, no. 16, p. 165401. doi: 10.1103/PhysRevB.65.165401.

[36] Sánchez-Portal D., Ordejon P., Artacho E., Soler, J.M. Density functional method for very large systems with LCAO basis sets. *International Journal of Quantum Chemistry*, 1997, vol. 65, no. 5, pp. 453–461. doi: 10.1002/(SICI)1097-461X(1997)65:5<453::AID-QUA9>3.0.CO;2-V.

[37] Weinert M., Wimmer E., Freeman A.J. Total-energy all-electron density functional method for bulk solids and surfaces. *Physical Review B*, 1982, vol. 26, no. 8, pp. 4571–4578.

[38] Grimme S., Antony J., Ehrlich S., Krieg H. A consistent and accurate ab initio parametrization of density functional dispersion correction (DFT-D) for the 94 elements H-Pu. *The Journal of Chemical Physics*, 2010, vol. 132, no. 15, p. 154104. doi: 10.1063/1.3382344.

[39] Lippert G., Hutter J., Parrinello M. The Gaussian and augmented-plane-wave density functional method for ab initio molecular dynamics simulations. *Theoretical Chemistry Accounts*, 1999, vol. 103, no. 2, pp. 124–140. doi: 10.1007/s002149900042.

[40] Mehl M.J., Klein B.M., Papaconstantopoulos D.A. First principles calculations of elastic properties of metals. *Intermetallic compounds: principles and applications*, 1994, vol. 1, pp. 195–210.

[41] Onuchina M.R., Artamonov A.A., Evdokimov V.B. Study of the lattice dynamics of B2 RuAl by the first principles methods. *Proceedings of VIAM*, 2018, no. 1(61), pp. 99–110. doi: 10.18577/2307-6046-2018-0-1-12-12.

[42] Giannozzi P., Baroni S., Bonini N., Calandra M., Car R., Cavazzoni C., Dal Corso A. QUANTUM ESPRESSO: a modular and open-source software project for quantum simulations of materials. *Journal of physics: Condensed matter*, 2009, vol. 21, no. 39, 19 p. Available at: http://stacks.iop.org/0953-8984/21/i=39/a=395502. doi: 10.1088/0953-8984/21/39/395502.

[43] Baroni S., Dal Corso A., de Gironcoli S., Giannozzi P., Cavazzoni C., Ballabio G., Laasonen K. Plane-wave self-consistent field. Available at: http://www.pwscf.org/.

[44] Scandolo S., Giannozzi P., Cavazzoni C., de Gironcoli S., Pasquarello A., Baroni S. First-principles codes for computational crystallography in the Quantum-ESPRESSO package. *Zeitschrift für Kristallographie-Crystalline Materials*, 2005, vol. 220, no. 5/6, pp. 574–579. doi: 10.1524/zkri.220.5.574.65062.

[45] Lejaeghere K., Bihlmayer G., Björkman T., Blaha P., Blügel S., Blum V., De Gironcoli S. Reproducibility in density functional theory calculations of solids. *Science*, 2016, vol. 351, no. 6280, aad3000. doi: 10.1126/science.aad3000.

[46] Matsushita T., Fecht H.J., Wunderlich R.K., Egry I., Seetharaman S. Studies of the thermophysical properties of commercial CMSX-4 alloy. *Journal of Chemical and Engineering Data*, 2009, vol. 54, no. 9, pp. 2584–2592. doi: 10.1021/je900132m.

[47] Blackman M. On the thermal expansion of solids. *Proceedings of the Physical Society. Section B*, 1957, vol. 70, no. 9, pp. 827–832. doi: 10.1088/0370-1301/70/9/303.

[48] Gilvarry J.J. Grüneisen parameter for a solid under finite strain. *Physical Review*, 1956, vol. 102, no. 2, p. 331. doi: 10.1103/PhysRev.102.331.

[49] Shang S.L., Wang Y., Kim D., Liu Z.K. First-principles thermodynamics from phonon and Debye model: Application to Ni and Ni3Al. *Computational Materials Science*, 2010, vol. 47, no. 4, pp. 1040–1048. doi: 10.1016/j.commatsci.2009.12.006.

[50] Lau S.F., Wunderlich B. Calculation of the heat capacity of linear macromolecules from theta-temperatures and group vibrations. *Journal of Thermal Analysis*, 1983, vol. 28, no.1, pp. 59–85.

[51] Morse P.M., Ingard K.U. *Theoretical acoustics*. Princeton, Princeton university press, 1986, 949 p.

[52] Suwardie J.H., Artiaga R., Mier J.L. Thermal characterization of a Ni-based superalloy. *Thermochimica Acta*, 2002, vol. 392–393, pp. 295–298. doi: 10.1016/S0040-6031(02)00112-0.

[53] D'Souza N., Dong H.B., Ardakani M.G., Shollock B.A. Solidification path in the Ni-base superalloy, IN713LC–quantitative correlation of last stage solidification. *Scripta Materialia*, 2005, vol. 53, no. 6, pp. 729–733. doi: 10.1016/j.scriptamat.2005.05.012.

[54] Zaretsky E.B., Kanel G.I., Razorenov S.V., Baumung K. Impact strength properties of nickel-based refractory superalloys at normal and elevated temperatures. *International Journal of Impact Engineering*, 2005, vol. 31, no. 1, pp. 41–54. doi: 10.1016/j.ijimpeng.2003.11.004.

[55] Zieliñska M., Yavorska M., Porêba M., Sieniawski J. Thermal properties of cast nickel based superalloys. *Archives of Materials Science and Engineering*, 2010, vol. 44, no.1, pp. 35–38.

[56] Lee S.H., Kim S.W., Kang K.H. Effect of heat treatment on the specific heat capacity of nickel-based alloys. *International Journal of Thermophysics*, 2006, vol. 27, no.1, pp. 282–292. doi: 10.1007/s10765-006-0029-2.

[57] Duane C.W. A Review of the Stratified Charge Engine Concept. *Physical Review,* 1965, vol. 37, no. 3A, pp. 37–43. doi: 10.1007/978-1-4757-9348-2_2.

[58] Chesnokov D.V., Antipov V.V., Kulushina N.V. The method of accelerated laboratory tests of aluminum alloys for determination of their corrosion resistance in conditions of the sea atmosphere. *Proceedings of VIAM*, 2016, no. 5(41), pp. 92–99. doi: 10.18577/2307-6046-2016-0-5-10-10. In Russian.

[59] Tryon B., Pollock T.M., Gigliotti M.F.X., Hemker K. Thermal expansion behavior of ruthenium aluminides. *Scripta Materialia*, 2004, vol. 50, no.6, pp. 845–848. doi: 10.1016/j.scriptamat.2003.12.009.

[60] Mücklich F., Ilić N., Woll K. RuAl and its alloys, Part II: Mechanical properties, environmental resistance and applications. *Intermetallics*, 2008, vol. 16, no. 5, pp. 593–608. doi: 10.1016/j.intermet.2008.02.010.

[61] Tryon B., Pollock T.M. Experimental assessment of the Ru–Al–Ni ternary phase diagram at 1000 and 1100 °C. *Materials Science and Engineering: A*, 2006, vol. 430, no. 1–2, pp. 266–276. doi: 10.1016/j.msea.2006.05.088.

[62] Mücklich F., Ilić N. RuAl and its alloys. Part I. Structure, physical properties, microstructure and processing. *Intermetallics*, 2005, vol. 13, no. 1, pp. 5–21. doi: 10.1016/j.intermet.2004.05.005.

[63] Gargano P., Mosca H., Bozzolo G., Noebe R.D. Atomistic modeling of RuAl and (RuNi)Al alloys. *Scripta Materialia*, 2003, vol. 48, no. 6, pp. 695–700. doi: 10.1016/S1359-6462(02)00556-0.

[64] Pan Y., Zhu J., Luo J. Role of Ru concentration on structure, mechanical and thermodynamic properties of Ru-Al compounds. *Materials and Design*, 2017, vol. 118, pp. 146–151. doi: 10.1016/j.matdes.2017.01.049.

[65] Pan Y., Jin C. Vacancy-induced mechanical and thermodynamic properties of B2-RuAl. *Vacuum*, 2017, vol. 143, pp. 165–168. doi: 10.1016/j.vacuum.2017.06.013.

[66] Tanaka K., Koiwa M. Elastic properties of high-temperature intermetallics. *High Temperature Materials and Processes*, 1999, vol. 18, no. 5–6, pp. 323–336. doi: 10.1515/HTMP.1999.18.5-6.323.

[67] Sot R., Kurzydlowski K.J. Atomic modelling of point defects in B2-RuAl. *Materials Science–Poland*, 2005, vol. 23, no. 2, pp. 407–411.

[68] Darolia R. NiAl alloys for high-temperature structural applications. *JoM*, 1991, vol. 43, no. 3, pp. 44–49. doi: 10.1007/BF03220163.

[69] Anderson S.A., Lang C.I. Thermal conductivity of ruthenium aluminide (RuAl). *Scripta Materialia*, 1998, vol. 38, no.3, pp. 493–497. doi: 10.1016/S1359-6462(97)00439-9.

[70] Pavlovskaya T.G., Deshevaya E.A., Zaitsev S.N., Kozlov I.A., Volkov I.A., Zakharov K.E. Corrosion resistance of aluminum alloys in conditions simulating the factors of space flight. *Proceedings of VIAM*, 2016, no. 3(39), pp. 85–93. doi: 10.18577/2307-6046-2016-0-3-11-11. In Russian.

[71] Morozova G.I. The importance of physicochemical phase analysis technique in the development of aviation metallic material science and creation of Ni-based superalloys (Dedicated to the 125th anniversary of the N.I. Blok's birth). *Proceedings of VIAM*, 2016, no. 1(37). doi: 10.18577/2307-6046-2016-0-1-50-55. In Russian.

[72] Artamonov A.A., Plotnikov E. Thermodynamic uncertainty relation as a fundamental aspect of quantum thermodynamics. *Resource-Efficient Technologies*, 2018, no. 1, pp. 17–29. doi: 10.18799/24056537/2018/1/178.

[73] Artamonov A.A., Plotnikov E.M. Thermodynamic and relativistic uncertainty relations. *Journal of Physics: Conference Series*, 2017, vol. 798, article number 012098. doi: 10.1088/1742-6596/798/1/012098.

Received: 10.03.2019